Nonlinear Engineering, Vol. **2** (2013), pp. 63–77 DOI 10.1515/nleng-2012-0011

An Efficient Motion Control System for Underwater Gliders

N. Mahmoudian[1,*] **and C. A. Woolsey**[2]

[1] Department of Mechanical Engineering - Engineering Mechanics, Michigan Technological University, Houghton MI 49931, USA

[2] Department of Aerospace and Ocean Engineering, Virginia Polytechnic Institute and State University, Blacksburg VA 24060, USA

Abstract. This paper describes an underwater glider motion control system intended to enhance locomotive efficiency by reducing the energy expended by vehicle guidance and control. In previous work, the authors obtained an approximate analytical expression for steady turning motion as a regular perturbation from wings level flight. Using this steady turn solution, one may easily construct feasible, energy-efficient paths for a glider to follow. Because the turning motion results are only approximate, however, and to compensate for model and environmental uncertainty, one must incorporate feedback to ensure precise path following. This paper describes the development and numerical implementation of a feedforward/feedback motion control system for a multi-body underwater glider model. The feedforward component issues actuator commands based on the analytical solution for a desired steady flight condition while the feedback component compensates for uncertainty and disturbances.

Keywords. Underwater glider, Motion control, Stability, Steady flight, Slowly varying system.

1 Introduction

Remote sensing from spacecraft aids ocean scientists by providing broad, dense measurements of ocean surface properties. However, only limited measurements under the ocean's surface can be made, typically with ocean profiling floats that drift with the currents. Marine scientists are beginning to rely more heavily on autonomous underwater vehicles (AUVs), however, to gather critical oceanographic data. An underwater glider is a special form of AUV that changes its buoyancy in order to sink and rise, while a fixed wing generates lift to propel the vehicle forward. The vehicle uses servo-actuators to shift its center of gravity (CG) relative to the center of buoyancy (CB) in order to control its pitch and roll attitude. By appropriately cycling these actuators, an underwater glider can control its flight path and propel itself with great efficiency. Because underwater gliders spend most of their time in stable, steady motion, expending control energy only when changing their equilibrium state, and because they are extremely robust, they have the capacity to stay in water for months collecting a large amount of horizontal and vertical in-situ data. For example, Rutgers University Coastal Ocean Observation Lab (RU-COOL) has flown battery powered *Slocum* Gliders over 62000 km in partnership with Teledyne Webb Research in different endurance flights [15]. (Figure 1 shows a solid model of the *Slocum* gilder.) The success of the first generation of underwater gliders including *Slocum* [30], *Seaglider* [5], and *Spray* [27] in deep sea exploration motivated a variety of new designs for different applications in shallow water ([33] and [31]).

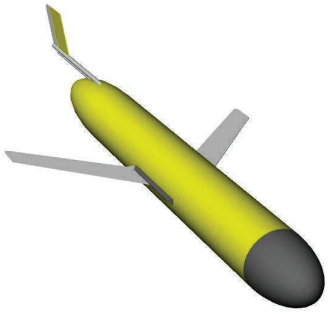

Figure 1. The underwater glider *Slocum* solid model in Rhinoceros 3.0 [9]
Mass 50 (kg); Length 1.5 (m); Wing Span 1 (m); Diameter 0.2 (m).

Extensive work regarding dynamics and control systems of Underwater Gliders has been developed [1, 2, 8, 10, 14]. With increased interest in using underwater gliders for littoral surveillance and military applications, stability and performance analysis of underwater gliders, particularly in turning motion, has been the subject of several papers [6,20,34]. Related research has focused on cooperative control of glider "schools" to improve measurement quality and robustness [19, 24, 28], as well as underwater localization, which is important in applications that require more precision than dead reckoning [3, 29].

In developing a feedback control law for an underwater glider, Leonard and Graver in [10, 18] mentioned the potential value of "complementing the feedback law with a feedforward term which drives the movable mass and the

Corresponding author: N. Mahmoudian, E-mail: ninam@mtu.edu.

Received: 12 July 2012. Accepted: 11 October 2012.

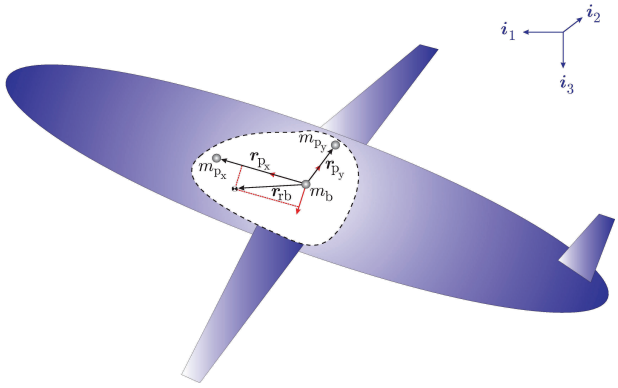

Figure 2. Illustration of point mass actuators.

variable mass in a predetermined way from initial to final condition." We consider a feedforward/feedback structure for the motion control system as explained in [23]. The feedforward term drives the servo-actuators and the buoyancy bladder to predetermined values obtained from the analytical solution presented in [20], corresponding to some desired steady flight condition. The feedback term compensates for the errors due to the approximation and environmental uncertainty. Steady motions can then be concatenated to achieve compatible guidance objectives, such as waypoint following.

Our aim is to develop implementable, energy-efficient motion control strategies that further improve the inherent efficiency of underwater gliders. Section 2 describes a general dynamic model for an underwater glider. Section 3 reviews the conditions for wings-level gliding flight given in [11] and the approximate conditions for steady turning flight developed in [20]. The motion control system design is presented in Sections 4 through 5 and the stability of the closed loop system is analyzed in Section 6. Simulation results for the *Slocum* model given in [2] are presented in Section 7. Conclusions of the work and a description of ongoing research are provided in Section 8.

2 Vehicle Dynamic Model with Actuator Dynamics

The glider is modeled as a rigid body (mass m_{rb}) with two moving mass actuators ($m_{\mathrm{p_x}}$ and $m_{\mathrm{p_y}}$) and a variable ballast actuator (m_{b}). The total vehicle mass is

$$m_{\mathrm{v}} = m_{\mathrm{rb}} + m_{\mathrm{p_x}} + m_{\mathrm{p_y}} + m_{\mathrm{b}},$$

where m_{b} can be modulated by control.

The vehicle displaces a volume of fluid of mass m. If $\tilde{m} := m_{\mathrm{v}} - m$ is greater than zero, the vehicle is heavy in water and tends to sink while if $\tilde{m}$ is negative, the vehicle is buoyant in water and tends to rise. Figure 2 shows the simplified model for the underwater glider actuation system. The variable mass is represented by a mass particle m_{b} located at the origin of a body-fixed reference frame.

The vehicle's attitude is given by a proper rotation matrix $\boldsymbol{\mathcal{R}}_{\mathrm{IB}}$ which maps free vectors from the body-fixed reference frame to a reference frame fixed in inertial space. The body frame is defined by an orthonormal triad $\{\boldsymbol{b}_1, \boldsymbol{b}_2, \boldsymbol{b}_3\}$, where $\boldsymbol{b}_1$ is aligned with the body's longitudinal axis. The origin of a body-fixed reference frame is located the center of volume of the vehicle as illustrated in Figure 2. The inertial frame is represented by an orthonormal triad $\{\boldsymbol{i}_1, \boldsymbol{i}_2, \boldsymbol{i}_3\}$, where $\boldsymbol{i}_3$ is aligned with the local direction of gravity. To define the rotation matrix explicitly, let vectors $\boldsymbol{e}_i$ define the standard basis for $\mathbb{R}^3$ for $i \in \{1, 2, 3\}$:

$$\boldsymbol{e}_1 = \begin{pmatrix} 1 \\ 0 \\ 0 \end{pmatrix}, \quad \boldsymbol{e}_2 = \begin{pmatrix} 0 \\ 1 \\ 0 \end{pmatrix}, \quad \text{and} \quad \boldsymbol{e}_3 = \begin{pmatrix} 0 \\ 0 \\ 1 \end{pmatrix}$$

Also, let the character $\hat{\cdot}$ denote the 3×3 skew-symmetric matrix satisfying $\hat{\boldsymbol{a}}\boldsymbol{b} = \boldsymbol{a} \times \boldsymbol{b}$ for 3-vectors $\boldsymbol{a}$ and $\boldsymbol{b}$. The rotation matrix $\boldsymbol{\mathcal{R}}_{\mathrm{IB}}$ is typically parameterized using the roll angle ϕ, pitch angle θ, and yaw angle ψ:

$$\boldsymbol{\mathcal{R}}_{\mathrm{IB}}(\phi, \theta, \psi) = e^{\widehat{\boldsymbol{e}_3}\psi} e^{\widehat{\boldsymbol{e}_2}\theta} e^{\widehat{\boldsymbol{e}_1}\phi}$$

where

$$e^{\boldsymbol{Q}} = \sum_{n=0}^{\infty} \frac{1}{n!} \boldsymbol{Q}^n \quad \text{for} \quad \boldsymbol{Q} \in \mathbb{R}^{n \times n}.$$

Let $\boldsymbol{v} = [u,\ v,\ w]^T$ represent the translational velocity and let $\boldsymbol{\omega} = [p,\ q,\ r]^T$ represent the rotational velocity of the underwater glider with respect to inertial space, where $\boldsymbol{v}$ and $\boldsymbol{\omega}$ are both expressed in the body frame. Letting $\boldsymbol{y}$ represent the position of the body frame origin with respect to the inertial frame, the vehicle kinematic equations are

$$\dot{\boldsymbol{y}} = \boldsymbol{\mathcal{R}}_{\mathrm{IB}} \boldsymbol{v} \tag{1}$$

$$\dot{\boldsymbol{\mathcal{R}}}_{\mathrm{IB}} = \boldsymbol{R}_{\mathrm{IB}} \hat{\boldsymbol{\omega}}. \tag{2}$$

In terms of these Euler angles, the kinematic equations (1) and (2) become, respectively,

$$\begin{pmatrix} \dot{x} \\ \dot{y} \\ \dot{z} \end{pmatrix} = \begin{pmatrix} \cos\theta\cos\psi & \sin\phi\sin\theta\cos\psi - \cos\phi\sin\psi & \cos\phi\sin\theta\cos\psi + \sin\phi\sin\psi \\ \cos\theta\sin\psi & \cos\phi\cos\psi + \sin\phi\sin\theta\sin\psi & -\sin\phi\cos\psi + \cos\phi\sin\theta\sin\psi \\ -\sin\theta & \sin\phi\cos\theta & \cos\phi\cos\theta \end{pmatrix} \begin{pmatrix} u \\ v \\ w \end{pmatrix}$$

$$\begin{pmatrix} \dot{\phi} \\ \dot{\theta} \\ \dot{\psi} \end{pmatrix} = \begin{pmatrix} 1 & \sin\phi\tan\theta & \cos\phi\tan\theta \\ 0 & \cos\phi & -\sin\phi \\ 0 & \sin\phi\sec\theta & \cos\phi\sec\theta \end{pmatrix} \begin{pmatrix} p \\ q \\ r \end{pmatrix}.$$

As indicated in Figure 2, the mass particle $m_{\mathrm{p_x}}$ is constrained to move along the longitudinal axis while the mass particle $m_{\mathrm{p_y}}$ is constrained to move along the lateral axis:

$$\boldsymbol{r}_{\mathrm{p_x}} = r_{\mathrm{p_x}}\boldsymbol{e}_1 \quad \text{and} \quad \boldsymbol{r}_{\mathrm{p_y}} = r_{\mathrm{p_y}}\boldsymbol{e}_2$$

Following [32], define the mass, inertia, and inertial coupling matrices for the combined rigid body/moving mass/variable ballast system as

$$\begin{aligned} \boldsymbol{I}_{\mathrm{rb/p/b}} &= \boldsymbol{I}_{\mathrm{rb}} - m_{\mathrm{p_x}}\hat{\boldsymbol{r}}_{\mathrm{p_x}}\hat{\boldsymbol{r}}_{\mathrm{p_x}} - m_{\mathrm{p_y}}\hat{\boldsymbol{r}}_{\mathrm{p_y}}\hat{\boldsymbol{r}}_{\mathrm{p_y}} \\ \boldsymbol{M}_{\mathrm{rb/p/b}} &= m_{\mathrm{v}}\mathbb{I} \\ \boldsymbol{C}_{\mathrm{rb/p/b}} &= m_{\mathrm{rb}}\hat{\boldsymbol{r}}_{\mathrm{rb}} + m_{\mathrm{p_x}}\hat{\boldsymbol{r}}_{\mathrm{p_x}} + m_{\mathrm{p_y}}\hat{\boldsymbol{r}}_{\mathrm{p_y}} \end{aligned}$$

where $\mathbb{I}$ represents the 3×3 identity matrix. The rigid body inertia matrix $\boldsymbol{I}_{\mathrm{rb}}$ represents the distribution of mass m_{rb} and is assumed to take the form

$$\boldsymbol{I}_{\mathrm{rb}} = \begin{pmatrix} I_{xx} & 0 & -I_{xz} \\ 0 & I_{yy} & 0 \\ -I_{xz} & 0 & I_{zz} \end{pmatrix}$$

where the off-diagonal terms in $\boldsymbol{I}_{\mathrm{rb}}$ arise, for example, from an offset center of mass $\boldsymbol{r}_{\mathrm{rb}} = [x_{\mathrm{rb}}, 0, z_{\mathrm{rb}}]^T$. It is notationally convenient to compile the various inertia matrices into the *generalized* inertia matrix $\mathbb{M}_{\mathrm{rb/p/b}}$.

$$\mathbb{M}_{\mathrm{rb/p/b}} = \begin{pmatrix} \boldsymbol{I}_{\mathrm{rb/p/b}} & \boldsymbol{C}_{\mathrm{rb/p/b}} & m_{\mathrm{p_x}}\hat{\boldsymbol{r}}_{\mathrm{p_x}}\boldsymbol{e}_1 & m_{\mathrm{p_y}}\hat{\boldsymbol{r}}_{\mathrm{p_y}}\boldsymbol{e}_2 \\ \boldsymbol{C}^T_{\mathrm{rb/p/b}} & \boldsymbol{M}_{\mathrm{rb/p/b}} & m_{\mathrm{p_x}}\boldsymbol{e}_1 & m_{\mathrm{p_y}}\boldsymbol{e}_2 \\ -m_{\mathrm{p_x}}\boldsymbol{e}_1^T\hat{\boldsymbol{r}}_{\mathrm{p_x}} & m_{\mathrm{p_x}}\boldsymbol{e}_1^T & m_{\mathrm{p_x}} & 0 \\ -m_{\mathrm{p_y}}\boldsymbol{e}_2^T\hat{\boldsymbol{r}}_{\mathrm{p_y}} & m_{\mathrm{p_y}}\boldsymbol{e}_2^T & 0 & m_{\mathrm{p_y}} \end{pmatrix}$$

The generalized *added* inertia matrix is composed of the added mass matrix $\boldsymbol{M}_{\mathrm{f}}$, the added inertia matrix $\boldsymbol{I}_{\mathrm{f}}$, and the added inertial coupling matrix $\boldsymbol{C}_{\mathrm{f}}$:

$$\mathbb{M}_{\mathrm{f}} = \begin{pmatrix} \boldsymbol{I}_{\mathrm{f}} & \boldsymbol{C}_{\mathrm{f}} & \mathbb{O}_{3\times2} \\ \boldsymbol{C}^T_{\mathrm{f}} & \boldsymbol{M}_{\mathrm{f}} & \mathbb{O}_{3\times2} \\ \mathbb{O}_{2\times3} & \mathbb{O}_{2\times3} & \mathbb{O}_{2\times2} \end{pmatrix}$$

The generalized added inertia matrix accounts for the energy necessary to accelerate the fluid around the vehicle as it rotates and translates. In notation similar to that defined by SNAME [7][1],

$$\left(\begin{array}{c|c} \boldsymbol{I}_{\mathrm{f}} & \boldsymbol{C}_{\mathrm{f}} \\ \hline \boldsymbol{C}^T_{\mathrm{f}} & \boldsymbol{M}_{\mathrm{f}} \end{array}\right) = -\left(\begin{array}{ccc:ccc} L_{\dot{p}} & L_{\dot{q}} & L_{\dot{r}} & L_{\dot{u}} & L_{\dot{v}} & L_{\dot{w}} \\ M_{\dot{p}} & M_{\dot{q}} & M_{\dot{r}} & M_{\dot{u}} & M_{\dot{v}} & M_{\dot{w}} \\ N_{\dot{p}} & N_{\dot{q}} & N_{\dot{r}} & N_{\dot{u}} & N_{\dot{v}} & N_{\dot{w}} \\ \hdashline X_{\dot{p}} & X_{\dot{q}} & X_{\dot{r}} & X_{\dot{u}} & X_{\dot{v}} & X_{\dot{w}} \\ Y_{\dot{p}} & Y_{\dot{q}} & Y_{\dot{r}} & Y_{\dot{u}} & Y_{\dot{v}} & Y_{\dot{w}} \\ Z_{\dot{p}} & Z_{\dot{q}} & Z_{\dot{r}} & Z_{\dot{u}} & Z_{\dot{v}} & Z_{\dot{w}} \end{array}\right)$$

[1] In SNAME notation, roll moment is denoted by $\boldsymbol{K}$ rather than $\boldsymbol{L}$

The generalized inertia for the vehicle/fluid system is

$$\mathbb{M} = \mathbb{M}_{\mathrm{rb/p/b}} + \mathbb{M}_{\mathrm{f}} = \begin{pmatrix} \boldsymbol{I} & \boldsymbol{C} & m_{\mathrm{p_x}}\hat{\boldsymbol{r}}_{\mathrm{p_x}}\boldsymbol{e}_1 & m_{\mathrm{p_y}}\hat{\boldsymbol{r}}_{\mathrm{p_y}}\boldsymbol{e}_2 \\ \boldsymbol{C}^T & \boldsymbol{M} & m_{\mathrm{p_x}}\boldsymbol{e}_1 & m_{\mathrm{p_y}}\boldsymbol{e}_2 \\ -m_{\mathrm{p_x}}\boldsymbol{e}_1^T\hat{\boldsymbol{r}}_{\mathrm{p_x}} & m_{\mathrm{p_x}}\boldsymbol{e}_1^T & m_{\mathrm{p_x}} & 0 \\ -m_{\mathrm{p_y}}\boldsymbol{e}_2^T\hat{\boldsymbol{r}}_{\mathrm{p_y}} & m_{\mathrm{p_y}}\boldsymbol{e}_2^T & 0 & m_{\mathrm{p_y}} \end{pmatrix} \tag{3}$$

where the inertia $\boldsymbol{I}$, mass $\boldsymbol{M}$, and coupling $\boldsymbol{C}$ matrices are defined as follows:

$$\begin{aligned} \boldsymbol{I} &= \boldsymbol{I}_{\mathrm{rb/p/b}} + \boldsymbol{I}_{\mathrm{f}} \\ \boldsymbol{M} &= \boldsymbol{M}_{\mathrm{rb/p/b}} + \boldsymbol{M}_{\mathrm{f}} \\ \boldsymbol{C} &= \boldsymbol{C}_{\mathrm{rb/p/b}} + \boldsymbol{C}_{\mathrm{f}} \end{aligned}$$

Let $\boldsymbol{p}_{\mathrm{sys}}$ represent the total linear momentum of the vehicle/fluid system and $\boldsymbol{h}_{\mathrm{sys}}$ represent the total angular momentum both expressed in the body frame. Let $\boldsymbol{p}_{\mathrm{p_x}}$ and $\boldsymbol{p}_{\mathrm{p_y}}$ represent the total translational momentum of the moving mass particles expressed in the body frame. Defining the generalized velocity $\boldsymbol{\eta} = (\ \boldsymbol{\omega}^T \quad \boldsymbol{v}^T \quad \dot{r}_{\mathrm{p_x}} \quad \dot{r}_{\mathrm{p_y}}\ )^T$ and the generalized momentum $\boldsymbol{\nu} = (\ \boldsymbol{h}_{\mathrm{sys}}^T \quad \boldsymbol{p}_{\mathrm{sys}}^T \quad p_{\mathrm{p_x}} \quad p_{\mathrm{p_y}}\ )^T$, we have

$$\boldsymbol{\nu} = \mathbb{M}\boldsymbol{\eta} \tag{4}$$

The dynamic equations in mixed momentum/velocity notation are

$$\begin{aligned} \dot{\boldsymbol{h}}_{\mathrm{sys}} =& \boldsymbol{h}_{\mathrm{sys}} \times \boldsymbol{\omega} + \boldsymbol{p}_{\mathrm{sys}} \times \boldsymbol{v} + (m_{\mathrm{rb}} g \boldsymbol{r}_{\mathrm{rb}} + m_{\mathrm{p_x}} g \boldsymbol{r}_{\mathrm{p_x}} + \\ & m_{\mathrm{p_y}} g \boldsymbol{r}_{\mathrm{p_y}}) \times (\boldsymbol{\mathcal{R}}_{\mathrm{IB}}^T \boldsymbol{i}_3) + \boldsymbol{T}_{\mathrm{visc}} \\ \dot{\boldsymbol{p}}_{\mathrm{sys}} =& \boldsymbol{p}_{\mathrm{sys}} \times \boldsymbol{\omega} + \tilde{m} g (\boldsymbol{\mathcal{R}}_{\mathrm{IB}}^T \boldsymbol{i}_3) + \boldsymbol{F}_{\mathrm{visc}} \\ \dot{p}_{\mathrm{p_x}} =& \boldsymbol{e}_1 \cdot \left(\boldsymbol{p}_{\mathrm{p_x}} \times \boldsymbol{\omega} + m_{\mathrm{p_x}} g (\boldsymbol{\mathcal{R}}_{\mathrm{IB}}^T \boldsymbol{i}_3) \right) + \tilde{u}_{\mathrm{p_x}} \\ \dot{p}_{\mathrm{p_y}} =& \boldsymbol{e}_2 \cdot \left(\boldsymbol{p}_{\mathrm{p_y}} \times \boldsymbol{\omega} + m_{\mathrm{p_y}} g (\boldsymbol{\mathcal{R}}_{\mathrm{IB}}^T \boldsymbol{i}_3) \right) + \tilde{u}_{\mathrm{p_y}} \\ \dot{m}_{\mathrm{b}} =& u_{\mathrm{b}} \end{aligned} \tag{5}$$

where the terms $\boldsymbol{T}_{\mathrm{visc}}$ and $\boldsymbol{F}_{\mathrm{visc}}$ represent external moments and forces which do not derive from scalar potential functions. These moments and forces include control moments, such as the yaw moment due to a rudder, and viscous forces, such as lift and drag.

The forces $\tilde{u}_{\mathrm{p_x}}$ and $\tilde{u}_{\mathrm{p_y}}$ can be chosen to cancel to remaining terms in the equations for $\dot{p}_{\mathrm{p_x}}$ and $\dot{p}_{\mathrm{p_y}}$, so that

$$\begin{aligned} \dot{p}_{\mathrm{p_x}} &= u_{\mathrm{p_x}} \\ \dot{p}_{\mathrm{p_y}} &= u_{\mathrm{p_y}}. \end{aligned}$$

The new inputs $u_{\mathrm{p_x}}$ and $u_{\mathrm{p_y}}$ may then be chosen to servo-actuate the point mass positions for attitude control, subject to limits on point mass position and velocity. (Physically, these actuators might each consist of a large mass $m_{\mathrm{p_x}}$ or $m_{\mathrm{p_y}}$ mounted on a power screw that is driven by a servomotor.) The mass flow rate u_{b} is chosen to servo-actuate the vehicle's net weight, again subject to control magnitude and rate limits. These magnitude and rate limits are significant for underwater gliders and must be considered in control design and analysis.

The viscous forces and moments are expressed in terms of the hydrodynamic angles

$$\alpha = \arctan\left(\frac{w}{u}\right) \qquad \text{and} \qquad \beta = \arcsin\left(\frac{v}{V}\right)$$

where $V = \|\boldsymbol{v}\|$. The viscous force and moment are most easily expressed in the "current" reference frame. This frame is related to the body frame through the proper rotation

$$\boldsymbol{\mathcal{R}}_{\mathrm{BC}}(\alpha, \beta) = e^{-\widehat{\boldsymbol{e}_2}\alpha} e^{\widehat{\boldsymbol{e}_3}\beta} = \begin{pmatrix} \cos\alpha\cos\beta & -\cos\alpha\sin\beta & -\sin\alpha \\ \sin\beta & \cos\beta & 0 \\ \sin\alpha\cos\beta & -\sin\alpha\sin\beta & \cos\alpha \end{pmatrix}.$$

For example, one may write

$$\boldsymbol{v} = \boldsymbol{\mathcal{R}}_{\mathrm{BC}}(\alpha, \beta)(V\boldsymbol{e}_1) = \begin{pmatrix} V\cos\alpha\cos\beta \\ V\sin\beta \\ V\sin\alpha\cos\beta \end{pmatrix}.$$

Following standard modeling conventions, we write

$$\boldsymbol{F}_{\mathrm{visc}} = -\boldsymbol{\mathcal{R}}_{\mathrm{BC}}(\alpha, \beta) \begin{pmatrix} \mathcal{D}(\alpha) \\ \mathcal{S}_\beta \beta + S_{\delta r}\delta r \\ \mathcal{L}_\alpha \alpha \end{pmatrix}$$

and

$$\boldsymbol{T}_{\mathrm{visc}} = \boldsymbol{D}_\omega \boldsymbol{\omega} + \begin{pmatrix} L_\beta \beta \\ M_\alpha \alpha \\ N_\beta \beta + N_{\delta r}\delta r \end{pmatrix}.$$

Equations (1), (2), and (5) completely describe the motion of an underwater glider in inertial space. In studying steady motions, we typically neglect the translational kinematics (1). Moreover, the structure of the dynamic equations (5) is such that we only need to retain a portion of the rotational kinematics (2). Given the "tilt" vector $\boldsymbol{\zeta} = \boldsymbol{\mathcal{R}}_{\mathrm{IB}}^T \boldsymbol{i}_3$ (i.e., the body frame unit vector pointing in the direction of gravity), and referring to equation (2), it is easy to see that $\dot{\boldsymbol{\zeta}} = \boldsymbol{\zeta} \times \boldsymbol{\omega}$. The reduced set of dynamic equations, with buoyancy control and moving mass actuator dynamics explicitly represented, are:

$$\begin{aligned} \dot{\boldsymbol{h}}_{\mathrm{sys}} =& \boldsymbol{h}_{\mathrm{sys}} \times \boldsymbol{\omega} + \boldsymbol{p}_{\mathrm{sys}} \times \boldsymbol{v} + (m_{\mathrm{rb}} g \boldsymbol{r}_{\mathrm{rb}} + m_{\mathrm{p_x}} g \boldsymbol{r}_{\mathrm{p_x}} + \\ & m_{\mathrm{p_y}} g \boldsymbol{r}_{\mathrm{p_y}}) \times \boldsymbol{\zeta} + \boldsymbol{T}_{\mathrm{visc}} \end{aligned}$$

$$\begin{aligned}\dot{\boldsymbol{p}}_{\text{sys}} &= \boldsymbol{p}_{\text{sys}} \times \boldsymbol{\omega} + \tilde{m} g \boldsymbol{\zeta} + \boldsymbol{F}_{\text{visc}} \\ \dot{\boldsymbol{\zeta}} &= \boldsymbol{\zeta} \times \boldsymbol{\omega} \\ \dot{p}_{\text{p}_x} &= u_{\text{p}_x} \\ \dot{p}_{\text{p}_y} &= u_{\text{p}_y} \\ \dot{m}_{\text{b}} &= u_{\text{b}}\end{aligned} \tag{6}$$

As mentioned previously, equations (6) are written in mixed velocity/momentum notation. To design a control system, we convert these into a consistent set of state variables by computing

$$\dot{\boldsymbol{\eta}} = \left[\mathbb{M}^{-1}\dot{\boldsymbol{\nu}} - \mathbb{M}^{-1}\dot{\mathbb{M}}\ \ \mathbb{M}^{-1}\boldsymbol{\nu}\right]_{\boldsymbol{\nu}=\mathbb{M}\boldsymbol{\eta}} \tag{7}$$

where $\dot{\mathbb{M}}$ is the time derivative of the generalized inertia:

$$\dot{\mathbb{M}} = \begin{pmatrix} \dot{\boldsymbol{I}} & \dot{\boldsymbol{C}} & m_{\text{p}_x}\dot{\hat{\boldsymbol{r}}}_{\text{p}_x}\boldsymbol{e}_1 & m_{\text{p}_y}\dot{\hat{\boldsymbol{r}}}_{\text{p}_y}\boldsymbol{e}_2 \\ \dot{\boldsymbol{C}}^T & \mathbb{O}_{3\times 3} & 0\boldsymbol{e}_1 & 0\boldsymbol{e}_2 \\ -m_{\text{p}_x}\boldsymbol{e}_1^T\dot{\hat{\boldsymbol{r}}}_{\text{p}_x} & 0\boldsymbol{e}_1^T & 0 & 0 \\ -m_{\text{p}_y}\boldsymbol{e}_2^T\dot{\hat{\boldsymbol{r}}}_{\text{p}_y} & 0\boldsymbol{e}_2^T & 0 & 0 \end{pmatrix}$$

with

$$\begin{aligned}\dot{\boldsymbol{I}} &= -m_{\text{p}_x}(\hat{\boldsymbol{r}}_{\text{p}_x}\dot{\hat{\boldsymbol{r}}}_{\text{p}_x} + \dot{\hat{\boldsymbol{r}}}_{\text{p}_x}\hat{\boldsymbol{r}}_{\text{p}_x}) - m_{\text{p}_y}(\hat{\boldsymbol{r}}_{\text{p}_y}\dot{\hat{\boldsymbol{r}}}_{\text{p}_y} + \dot{\hat{\boldsymbol{r}}}_{\text{p}_y}\hat{\boldsymbol{r}}_{\text{p}_y}) \\ \dot{\boldsymbol{C}} &= m_{\text{p}_x}\dot{\hat{\boldsymbol{r}}}_{\text{p}_x} + m_{\text{p}_y}\dot{\hat{\boldsymbol{r}}}_{\text{p}_y}.\end{aligned}$$

3 Steady Flight

In wings-level, gliding flight the vehicle has zero angular velocity ($\boldsymbol{\omega} = \boldsymbol{0}$), zero lateral velocity component ($v = 0$, so that $\beta = 0$), and zero roll angle ($\phi = 0$). Also, $r_{\text{p}_y} = 0$ and $\delta r = 0$ (if the vehicle has a rudder). Following the analysis presented in [11], one may compute the required CG location ($\boldsymbol{r}_{\text{rb}}$) and the required net mass $\tilde{m}_0$ for balanced gliding flight at a specified speed and glide path angle. Let γ denote the glide path angle; in wings-level flight, $\gamma = \theta - \alpha$. For steady wings-level flight at a specified speed V_0 and glide path angle $\gamma_0 = \theta_0 - \alpha_0$,

$$\boldsymbol{r}_{\text{rb}} = \frac{1}{m_{\text{rb}} g}\left(\boldsymbol{M}\boldsymbol{v}_0 \times \boldsymbol{v}_0 + \begin{pmatrix} 0 \\ M_\alpha \alpha_0 \\ 0 \end{pmatrix}\right) \times \boldsymbol{\zeta}_0 + \varrho\boldsymbol{\zeta}_0 \tag{8}$$

$$\tilde{m}_0 = \frac{1}{g}\left(\cos(\gamma_0)\mathcal{L}_\alpha\alpha_0 - \sin(\gamma_0)\mathcal{D}(\alpha_0, 0)\right). \tag{9}$$

In the equation for $\boldsymbol{r}_{\text{rb}}$, $\boldsymbol{v}_0 = V_0\left[\cos\alpha_0,\ 0,\ \sin\alpha_0\right]^T$, $\boldsymbol{\zeta}_0 = \left[-\sin\theta_0,\ 0,\ \cos\theta_0\right]^T$, and ϱ is a free parameter related to the vehicle's "bottom-heaviness" in the given flight condition [11]. (Note that, in determining a nominal wings-level glide condition, we assume that $r_{\text{p}_x} = 0$. That is, the nominal gravitational moment is due entirely to $\boldsymbol{r}_{\text{rb}}$.) Analysis of turning (helical) flight using a sophisticated underwater glider model is challenging. In [22], the problem was formulated as a regular perturbation problem in the turn rate, as represented by a small, non-dimensional turn rate parameter ϵ. In seeking a first order solution for turning flight, it was assumed that the pitch angle remains at its nominal value for wings-level flight (θ_0). Polynomial expansions for V, α, β, r_{p_y}, $\tilde{m}$, and ϕ in terms of ϵ were substituted into the nonlinear algebraic equations for steady turning flight. (For example, one writes $V = V_0 + \epsilon V_1 + \epsilon^2 V_2 + \ldots$, where V_0 is the nominal speed in wings level flight.) Solving the coefficient equations for ϵ^1 gives approximate equilibrium values for r_{p_y}, $\tilde{m}$, ϕ, V, α, and β, to first order in ϵ. It was found in [22] that these first order approximate values take the form:

$$\begin{aligned} V_1 &= 0 \\ \alpha_1 &= 0 \\ \tilde{m}_1 &= 0 \\ \beta_1 &= \beta_1(\alpha_0, \theta_0, \tilde{m}_0; \delta_{r_1}) \\ \phi_1 &= \phi_1(\alpha_0, \theta_0, \tilde{m}_0; \beta_1, \delta_{r_1}) \\ r_{\text{p}_{y_1}} &= r_{\text{p}_{y_1}}(\alpha_0, \theta_0, \tilde{m}_0; \delta_{r_1}) \end{aligned} \tag{10}$$

Explicit expressions for β_1, ϕ_1, and $r_{\text{p}_{y_1}}$ are given in [22]. The approximate solution indicated in (10) shows that V, α, and $\tilde{m}$ remain constant to first order in ϵ. This suggests that the primary contributors to steady turning motion are lateral mass deflections (r_{p_y}) and rudder deflections (δr), if a rudder is present, and that these deflections have no first order effect on speed or angle of attack. In practice, it is considerably more costly to change the vehicle's net mass $\tilde{m}$ than to shift its CG, so it is fortunate that turning motions at the same (approximate) speed and glide path angle can be obtained by only varying r_{p_y} and/or δ_r. These observations suggest a natural approach to motion control for underwater gliders: Fix the buoyancy and center of gravity for a desired, wings level flight condition and then use the lateral moving mass actuator to control turn rate and longitudinal moving mass actuator to control flight path angle.

4 Motion Control System

Having characterized steady, wings level flight and steady turning motions (at least approximately), as described in Section 3, one can formulate a motion control strategy which relies on these solutions. The aim is to track inputs of constant desired speed (V_{d}), glide path angle (γ_{d}), and turn rate ($\dot{\psi}_{\text{d}}$). Given feasible values for desired speed, glide path angle, and turn rate, one may compute feedforward actuator commands to adjust the net weight and cen-

ter of gravity in order to achieve the given flight condition. Because these values are only approximate, though, and because of modeling and environmental uncertainty, the commanded values must be augmented using feedback compensation. The design and analysis of such a feedforward/feedback motion control system requires a model that incorporates buoyancy and moving mass actuator dynamics as presented in Section 2.

An illustration of such a feedforward/feedback control system is shown in Figure 3. The vector field $\boldsymbol{f}(\boldsymbol{x}, \boldsymbol{u})$ represents the system dynamics with state vector $\boldsymbol{x}$ and inputs $\boldsymbol{u}$, and the vector field $\tilde{\boldsymbol{f}}(\boldsymbol{x}, \boldsymbol{u})$ notionally represents their first order approximation in turn rate. The pair $(\tilde{\boldsymbol{x}}_{\text{eq}}, \tilde{\boldsymbol{u}}_{\text{eq}})$ represents the first order solution for a given desired steady motion. The vector $\boldsymbol{\mu}$ contains parameter values which, if held constant, correspond to some stable steady motion. Such a feedforward/feedback motion control system was briefly presented in [23]; a more thorough discussion of the design and analysis was presented [21].

The first step in the motion control scheme is to obtain the parameter values $\tilde{\boldsymbol{\mu}}_{\text{d}}$ (net mass and moving mass positions) that correspond to the desired steady motion $\tilde{\boldsymbol{x}}_{\text{eq}}$ (characterized by V_{d}, γ_{d}, and $\dot{\psi}_{\text{d}}$), to first order in turn rate. This inverse problem is expressed notationally in the feedforward block in Figure 3 by the equation

$$\mathbf{0} = \tilde{\boldsymbol{f}}(\tilde{\boldsymbol{x}}_{\text{eq}}, \tilde{\boldsymbol{u}}_{\text{eq}}),$$

which was solved analytically for the corresponding parameter values $\tilde{\boldsymbol{\mu}}_{\text{d}}$ in [22].

The feedback block compensates for the error due to the approximation and environmental uncertainty, adding a correction denoted $\boldsymbol{\mu}^{\text{corr}}$.

The feedback-compensated "parameter commands" $\boldsymbol{\mu}_{\text{d}}$ are then realized within the vehicle dynamics

$$\dot{\boldsymbol{x}} = \boldsymbol{f}(\boldsymbol{x}; \boldsymbol{u}(\boldsymbol{x}; \boldsymbol{\mu}_{\text{d}}))$$

through an appropriately designed servo-control system. Here, $\boldsymbol{u}$ is a feedback control law that attempts to maintain commanded parameter values $\boldsymbol{\mu}_{\text{d}}$ in spite of the vehicle dynamics.

The control system depicted in Figure 3 suggests that one may vary the steady motion, according to some desired guidance objective. However, one must verify that the closed loop system is stable. Fixing parameter values, one may examine open-loop stability by linearizing about the approximate equilibrium conditions and computing the eigenvalues of the state matrix. Because eigenvalues depend continuously on the matrix parameters, stability of the true equilibrium may be inferred from stability of the approximate equilibrium provided (i) the equilibrium is hyperbolic and (ii) ϵ is small relative to the magnitude of the real part of each eigenvalue. See Section 1.7 of [12] for a brief discussion or Chapter 9 of [13] for more details. While the system does possess a stable, steady motion parameterized by a set of commanded parameter values, one must still verify that the system remains stable while varying these parameter values. For example, if one changes the reference commands in Figure 3 too rapidly, one might drive the nonlinear system unstable.

As explained earlier, underwater gliders steer by moving one or more internal masses. The vehicle dynamics are quite slow, relative to the actuator dynamics. Commanding a rapid change in turn rate, for example, will result in a quick change in center of mass location, but the resulting effect on the vehicle's motion will be much slower. Alternatively, one may issue reference commands that vary "quasisteadily" and treat the closed-loop system as "slowly varying" in the turn rate $\dot{\psi}_{\text{d}}(t)$. We may then analyze stability of the closed loop system in the context of slowly varying systems theory [16].

Suppose the output of a nonlinear system

$$\dot{\boldsymbol{x}} = \boldsymbol{f}(\boldsymbol{x}, u_{\text{py}}); \quad u_{\text{py}} = \kappa(\boldsymbol{x}, \dot{\psi}_{\text{d}})$$

is required to track a reference input $\dot{\psi}_{\text{d}}(t)$, where the feedback controller κ is designed such that the closed-loop system has a locally exponentially stable equilibrium at $\boldsymbol{x}_{\text{eq}}$ when $\dot{\psi}_{\text{d}}(t)$ is constant. The turn rate $\dot{\psi}_{\text{d}}(t)$ is called "slowly varying" if it is continuously differentiable and, for some sufficiently small $\varepsilon > 0$, one has $\|\ddot{\psi}_{\text{d}}(t)\| \leq \varepsilon$ for all $t \geq 0$.

We will analyze the underwater glider's motion control system using slowly varying systems theory to prove stability of the closed-loop system and, simultaneously, to determine a (possibly conservative) bound on how fast one may vary the commanded turn rate and maintain stability.

Following Khalil [16, Ch. 9], to analyze this system, consider $\dot{\psi}_{\text{d}}$ as a "frozen" parameter and assume that for each fixed value the frozen system has an isolated equilibrium point defined by $\boldsymbol{x}_{\text{eq}} = \mathbf{h}(\dot{\psi}_{\text{d}})$ where $\|\frac{\partial \mathbf{h}}{\partial \dot{\psi}_{\text{d}}}\| \leq L$. To analyze stability of the frozen equilibrium point, we shift it to the origin via the change of the variables $\acute{\boldsymbol{x}} = \boldsymbol{x} - \mathbf{h}(\dot{\psi}_{\text{d}})$ to obtain equation

$$\dot{\acute{\boldsymbol{x}}} = \boldsymbol{g}(\acute{\boldsymbol{x}})$$

Based on Theorem 9.3 in [16], if there is a positive definite and decrescent Lyapunov function $V(\acute{\boldsymbol{x}})$ that has a negative definite derivative along the trajectories of the system and which satisfies certain inequalities to handle the perturbation and the fact that $\dot{\psi}_{\text{d}}(t)$ is not constant, the solution will be uniformly ultimately bounded within a ball around the equilibrium point, with a radius proportional to ε, for sufficiently small ε. Moreover, if $\ddot{\psi}_{\text{d}}(t) \to 0$ as $t \to \infty$, then the tracking error tends to zero. As will be discussed in Section 6, the resulting ε may be conservative.

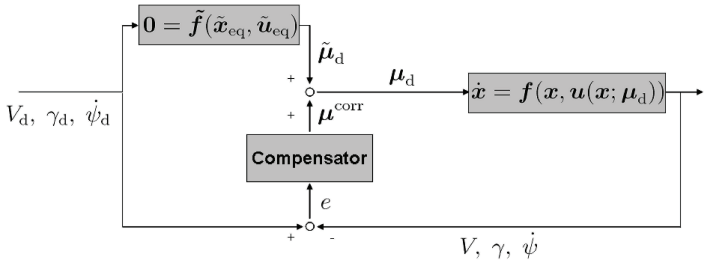

Figure 3. A steady motion-based feedforward/feedback control system.

5 Feedforward/Feedback Controller Design

The feedforward block takes the commanded steady motion parameters (speed, glide path angle, and turn rate) and generates the corresponding values for buoyancy and center of mass location, as predicted by perturbation analysis. Because the turning motion results are only approximate, however, and to compensate for model and environmental uncertainty, we incorporate feedback. The objective here is to design single-input, single-output PID control loops to *modify* the feedforward commands based on measured errors in the values of speed V, glide path angle $\gamma = \theta - \alpha$, and heading rate $\dot{\psi} = \frac{\sin\phi}{\cos\theta} q + \frac{\cos\phi}{\cos\theta} r$. Speed and glide path angle are inherently coupled for underwater gliders, just as they are for airplanes. For a *fixed* glide path angle, speed can be directly modulated by changing the net mass $\tilde{m}$. Changing $\tilde{m}$ requires pressure-volume work, however, which is relatively expensive, especially at depth. In practice, it is best to modulate $\tilde{m}$ as infrequently as possible. Here, we focus on controlling the glide path angle γ by varying the longitudinal moving mass position $r_{\rm p_x}$.

A sophisticated dynamic model presented in Section 2 has been used to design the feedback compensator. The model incorporates the buoyancy and moving mass actuator dynamics and servo-control laws. It is convenient to replace the velocity $\boldsymbol{v}$, as expressed in the body reference frame, with speed, angle of attack, and sideslip angle (V, α, β). To do so, note that

$$
\begin{aligned}
\boldsymbol{v} &= e^{-\widehat{\boldsymbol{e}}_2\alpha} e^{\widehat{\boldsymbol{e}}_3\beta} (V \boldsymbol{e}_1) \\
\dot{\boldsymbol{v}} &= e^{-\widehat{\boldsymbol{e}}_2\alpha} e^{\widehat{\boldsymbol{e}}_3\beta} \begin{pmatrix} 1 & 0 & 0 \\ 0 & 0 & V \\ 0 & V\cos\beta & 0 \end{pmatrix} \begin{pmatrix} \dot{V} \\ \dot{\alpha} \\ \dot{\beta} \end{pmatrix}.
\end{aligned}
$$

The change of variables is well-defined for $\beta \in (-\frac{\pi}{2}, \frac{\pi}{2})$.

The equations of motion (7) can be written in the form

$$
\mathbb{F}(\dot{\mathbb{X}}, \mathbb{X}, \mathbb{U}) = \mathbf{0}
$$

where the system state and control vectors are

$$
\begin{aligned}
\mathbb{X} &= \left[\phi, \theta, V, \alpha, \beta, p, q, r, r_{\rm p_x}, v_{\rm p_x}, r_{\rm p_y}, v_{\rm p_y}\right]^T \\
\mathbb{U} &= \left[u_{\rm p_x}, u_{\rm p_y}, u_{\rm b}\right]^T.
\end{aligned}
$$

Note that $v_{\rm p_x}$ and $v_{\rm p_y}$ represent the translational velocity of the moving masses relative to the inertial frame expressed in the body frame.

To design a servo-controller for the moving mass actuators and the variable ballast actuator, we linearize the dynamic equations about a wings-level equilibrium $(\mathbb{X}_0, \mathbb{U}_0)$ and compute the transfer function for each input-output channel of interest. Let U denote one of the available input signals $U \in \left\{u_{\rm p_x}, u_{\rm p_y}, u_{\rm b}\right\}$ and define a corresponding output $Y(\mathbb{X})$. With these definitions, we obtain the perturbation equations

$$
\begin{aligned}
\triangle\dot{\mathbb{X}} &= \boldsymbol{A}\triangle\mathbb{X} + \boldsymbol{B}\triangle U \qquad (11) \\
\triangle Y &= \boldsymbol{C}\triangle\mathbb{X} \qquad (12)
\end{aligned}
$$

where

$$
\begin{aligned}
\boldsymbol{A} &= -\left[\left(\frac{\partial\mathbb{F}}{\partial\dot{\mathbb{X}}}\right)^{-1}\left(\frac{\partial\mathbb{F}}{\partial\mathbb{X}}\right)\right]_{\rm eq} \\
\boldsymbol{B} &= -\left[\left(\frac{\partial\mathbb{F}}{\partial\dot{\mathbb{X}}}\right)^{-1}\left(\frac{\partial\mathbb{F}}{\partial U}\right)\right]_{\rm eq} \\
\boldsymbol{C} &= \left[\frac{\partial Y}{\partial\mathbb{X}}\right]_{\rm eq}
\end{aligned}
$$

The matrix $\frac{\partial\mathbb{F}}{\partial\dot{\mathbb{X}}}$ is non-singular within the vehicle's normal performance envelope.

In designing moving mass servos, the objective is to choose an input $u_{\rm p} \in \{u_{\rm p}x, u_{\rm p_y}\}$ such that the position of the moving mass $r_{\rm p} \in \{r_{\rm p}x, r_{\rm p_y}\}$ asymptotically tracks a desired trajectory $r_{\rm p_d} \in \{r_{\rm p}x_{\rm d}, r_{\rm p_y d}\}$. With $U = u_{\rm p}$ and $Y = r_{\rm p}$ in equations (11) and (12), the scalar $\boldsymbol{CAB}$ is nonzero. Let $e = r_{\rm p_d} - r_{\rm p}$ represent the error between the desired position of a moving mass and its current position. In order to drive e to zero, one may choose

$$
u_{\rm p} = \frac{1}{\mathbf{CAB}}(\ddot{r}_{\rm p_d} - \mathbf{CA}^2\triangle\mathbb{X} + [\omega_{\rm n}^2 \;\; 2\zeta\omega_{\rm n}]\mathbf{e})
$$

where $\mathbf{e} = [e, \dot{e}]^T$ and where $\omega_{\rm n} \in \{\omega_{\rm n}x, \omega_{\rm n_y}\}$ and $\zeta \in \{\zeta_x, \zeta_y\}$ are appropriately chosen control parameters, assuming that $r_{\rm p_d}$ is twice differentiable.

To design a PID compensator to correct the feedforward commands, let $G(s)$ represent the transfer function for a particular control channel and let $G_c(s)$ represent the PID controller:

$$G_c(s) = K_p(1 + \frac{1}{T_i s} + T_d s)$$

The proportional gain K_p, the integrator time T_i and the derivative time T_d are control parameters to be tuned by the control designer. In the time domain, the control signal is

$$r_{\mathrm{p}}^{\mathrm{corr}} = K_p e + K_i \int_{t_0}^{t} e(\tau) d\tau + K_d \dot{e}$$

where $K_i = K_p/T_i$ and $K_d = K_p T_d$. The error signal $e(t)$ measures the difference between the actual and commanded value of the output.

The approximate equilibrium value of $\tilde{r}_{\mathrm{p_d}} \in \{\tilde{r}_{\mathrm{p}x_{\mathrm{d}}}, \tilde{r}_{\mathrm{p}y_{\mathrm{d}}}\}$, as predicted by analytical solutions, is augmented with feedback compensation to correct for approximation error:

$$r_{\mathrm{p_d}} \quad = \quad \tilde{r}_{\mathrm{p_d}} + r_{\mathrm{p}}^{\mathrm{corr}}.$$

To smooth the commanded parameter value so that the reference command to the internal servo-actuators is twice differentiable, we define a linear reference model:

$$F(s) : r_{\mathrm{p_d}} \rightarrow r_{\mathrm{p_d}}^{\mathrm{comm}}$$

where

$$F(s) = \frac{1}{(s/\omega_{\mathrm{r}})^2 + 2\zeta_{\mathrm{r}}(s/\omega_{\mathrm{r}}) + 1}$$

Equivalently, in time domain, define the following reference model dynamics for each servo-actuator:

$$\begin{aligned} \dot{\mathbf{z}} &= \begin{pmatrix} 0 & 1 \\ -\omega_{\mathrm{r}}^2 & -2\zeta_{\mathrm{r}}\omega_{\mathrm{r}} \end{pmatrix} \mathbf{z} + \begin{pmatrix} 0 \\ \omega_{\mathrm{r}}^2 \end{pmatrix} r_{\mathrm{p_d}} \\ r_{\mathrm{p_d}}^{\mathrm{comm}} &= \begin{pmatrix} 1 & 0 \end{pmatrix} \mathbf{z} \end{aligned}$$

where $r_{\mathrm{p_d}}(t) \in \{r_{\mathrm{p}x_{\mathrm{d}}}(t), r_{\mathrm{p}y_{\mathrm{d}}}(t)\}$ is the (possibly discontinuous) reference command to be filtered.

In physical implementations, the servo-actuation system is self-contained and there is no need to include it in the motion control system. Referring to the control system schematic in Figure 3, this reference command filter is internal to the system dynamics block appearing at the right. We include this element explicitly here in order to account for the full complexity of the multi-body mechanical system and to allow analysis of issues such as actuator magnitude and rate saturation. The natural frequency and damping ratio parameters in the reference model are chosen to respect actuator performance limits.

For a *fixed* glide path angle, speed can be directly modulated by changing the net mass $\tilde{m}$. That is, given values θ_0 and γ_0, one may solve relation (9) for the corresponding values of $\tilde{m}_{\mathrm{d}}$. We design an input u_{b} such that the net mass $\tilde{m}$ asymptotically tracks a desired value $\tilde{m}_{\mathrm{d}}$. The simplest approach is to choose

$$u_{\mathrm{b}} = k_{\mathrm{b}} (\tilde{m}_{\mathrm{d}} - \tilde{m})$$

where the constant k_{b} is chosen to accommodate the rate limit on u_{b}.

5.1 Flight Path Control

We control the glide path angle γ by modulating the longitudinal moving mass position $r_{\mathrm{p_x}}$. Let $e_\gamma(t) = \gamma_{\mathrm{d}} - \gamma(t)$, where γ_{d} is the desired value of the glide path angle. The longitudinal moving mass reference signal is

$$r_{\mathrm{p_x}}^{\mathrm{corr}} = K_{p_\gamma} e_\gamma + K_{i_\gamma} \int_{t_0}^{t} e_\gamma(\tau) d\tau + K_{d_\gamma} \dot{e}_\gamma.$$

The first step is to tune the flight path controller for the linearized system dynamics. Having done so, the next step is to re-tune the controller as necessary for the nonlinear dynamics through simulation. Adding the result to the longitudinal moving mass position from the feedforward block gives the required position of the longitudinal moving mass to maintain a constant flight path angle.

$$r_{\mathrm{p}x_{\mathrm{d}}} \quad = \quad \tilde{r}_{\mathrm{p}x_{\mathrm{d}}} + r_{\mathrm{p_x}}^{\mathrm{corr}}$$

As explained in Section 3, we have assumed that the nominal gravitational moment is due entirely to $\mathbf{r}_{\mathrm{rb}}$ and that $\tilde{r}_{\mathrm{p}x_{\mathrm{d}}} = 0$. Hence, for $\gamma_{\mathrm{d}} = \gamma_0$, we have only the feedback term $r_{\mathrm{p}x_{\mathrm{d}}} = r_{\mathrm{p_x}}^{\mathrm{corr}}$.

The reference command should be filtered to accommodate the magnitude and rate limit on the longitudinal moving mass actuator due to limited range of travel of the moving mass and the operational limit of the servomotor driving it.

$$r_{\mathrm{p}x_{\mathrm{d}}}^{\mathrm{comm}} \quad = \quad \begin{pmatrix} 1 & 0 \end{pmatrix} \mathbf{z}_{\mathrm{x}}$$

where

$$\dot{\mathbf{z}}_{\mathrm{x}} = \begin{pmatrix} 0 & 1 \\ -\omega_{\mathrm{r_x}}^2 & -2\zeta_{\mathrm{r_x}}\omega_{\mathrm{r_x}} \end{pmatrix} \mathbf{z}_{\mathrm{x}} + \begin{pmatrix} 0 \\ \omega_{\mathrm{r_x}}^2 \end{pmatrix} r_{\mathrm{p}x_{\mathrm{d}}}(t)$$

The input $u_{\mathrm{p_x}}$ guarantees that the position of the longitudinal moving mass $r_{\mathrm{p_x}}$ asymptotically tracks the twice differentiable trajectory $r_{\mathrm{p}x_{\mathrm{d}}}^{\mathrm{comm}}$ generated by filtering the desired value $r_{\mathrm{p}x_{\mathrm{d}}}$:

$$u_{\mathrm{p_x}} = \frac{(\ddot{r}_{\mathrm{p}x_{\mathrm{d}}}^{\mathrm{comm}} - \boldsymbol{C}_{\mathrm{x}} \boldsymbol{A}^2 \boldsymbol{X} + [\omega_{\mathrm{n_x}}^2 \;\; 2\zeta_{\mathrm{x}}\omega_{\mathrm{n_x}}]\mathbf{e}_{\mathrm{x}})}{\boldsymbol{C}_{\mathrm{x}} \boldsymbol{A} \boldsymbol{B}_{\mathrm{x}}}$$

where

$$\boldsymbol{e}_{\mathrm{x}} = (e_{\mathrm{x}}, \dot{e}_{\mathrm{x}})^T \qquad \text{and} \qquad e_{\mathrm{x}} = r^{\mathrm{comm}}_{\mathrm{p_{x_d}}} - r_{\mathrm{p_x}}$$

5.2 Turn Rate Control

The channel from lateral mass position $r^{\mathrm{corr}}_{\mathrm{p_y}}$ to turn rate $\dot{\psi}$ is non-minimum phase, with a single zero in the right half plane. This non-minimum phase zero limits closed-loop bandwidth. In any case, closing the loop from turn rate to lateral mass location is quite effective, provided the performance limitations are respected in control parameter selection. Let $e_{\dot{\psi}}(t) = \dot{\psi}_{\mathrm{d}}(t) - \dot{\psi}(t)$, where $\dot{\psi}_{\mathrm{d}}(t)$ is the desired turn rate. The lateral moving mass control signal is

$$r^{\mathrm{corr}}_{\mathrm{p_y}} = K_{p_{\dot{\psi}}} e_{\dot{\psi}} + K_{i_{\dot{\psi}}} \int_{t_0}^{t} e_{\dot{\psi}}(\tau) d\tau + K_{d_{\dot{\psi}}} \dot{e}_{\dot{\psi}}.$$

The turn rate PID controller was first tuned for the linearized system dynamics, and then re-tuned for the nonlinear dynamics through simulation. Adding the result to the lateral moving mass position from the feedforward block gives the required position of the lateral moving mass to maintain the desired turn rate.

$$r_{\mathrm{p_{y_d}}} = \tilde{r}_{\mathrm{p_{y_d}}} + r^{\mathrm{corr}}_{\mathrm{p_y}}$$

The reference command should be filtered, with filter parameters chosen in a way that respects the performance limitations (e.g., the rate limit) of the servomotor:

$$r^{\mathrm{comm}}_{\mathrm{p_{y_d}}} = \begin{pmatrix} 1 & 0 \end{pmatrix} \mathbf{z}_{\mathrm{y}}$$

where

$$\dot{\mathbf{z}}_{\mathrm{y}} = \begin{pmatrix} 0 & 1 \\ -\omega^2_{\mathrm{r_y}} & -2\zeta_{\mathrm{r_y}}\omega_{\mathrm{r_y}} \end{pmatrix} \mathbf{z}_{\mathrm{y}} + \begin{pmatrix} 0 \\ \omega^2_{\mathrm{r_y}} \end{pmatrix} r_{\mathrm{p_{y_d}}}(t)$$

The input $u_{\mathrm{p_y}}$ guarantees that the position of the lateral moving mass $r_{\mathrm{p_y}}$ asymptotically tracks the trajectory $r^{\mathrm{comm}}_{\mathrm{p_{y_d}}}$ generated by filtering the desired value $r_{\mathrm{p_{y_d}}}$:

$$u_{\mathrm{p_y}} = \frac{(\ddot{r}^{\mathrm{comm}}_{\mathrm{p_{y_d}}} - \boldsymbol{C}_{\mathrm{y}}\boldsymbol{A}^2\boldsymbol{X} + [\omega^2_{\mathrm{n_y}} \;\; 2\zeta_{\mathrm{y}}\omega_{\mathrm{n_y}}]\mathbf{e}_{\mathrm{y}})}{\boldsymbol{C}_{\mathrm{y}}\boldsymbol{A}\boldsymbol{B}_{\mathrm{y}}}$$

where

$$\boldsymbol{e}_{\mathrm{y}} = (e_{\mathrm{y}}, \dot{e}_{\mathrm{y}})^T \qquad \text{and} \qquad e_{\mathrm{y}} = r^{\mathrm{comm}}_{\mathrm{p_{y_d}}} - r_{\mathrm{p_y}}$$

6 Stability Analysis of Closed Loop System

To analyze this system, consider $\dot{\psi}_{\mathrm{d}}$ as a "frozen" parameter. For each fixed value the frozen system has an isolated equilibrium point. Consider the linearized equations about this equilibrium point:

$$\begin{aligned} \dot{\mathbb{X}} &= \boldsymbol{A}\mathbb{X} + \boldsymbol{B}_{\mathrm{y}} u_{\mathrm{p_y}} \\ r_{\mathrm{p_y}} &= \boldsymbol{C}_{\mathrm{y}}\mathbb{X} \end{aligned}$$

where $\mathbb{X}$ is the state vector

$$\mathbb{X} = \left[\phi, \theta, V, \alpha, \beta, p, q, r, r_{\mathrm{p_x}}, v_{\mathrm{p_x}}, r_{\mathrm{p_y}}, v_{\mathrm{p_y}}\right]^T$$

Defining the lateral mass error $e_{\mathrm{y}} = r^{\mathrm{comm}}_{\mathrm{p_{y_d}}} - r_{\mathrm{p_y}}$ and the heading rate error $e_{\dot{\psi}} = \dot{\psi}_{\mathrm{d}} - \dot{\psi}$, the input $u_{\mathrm{p_y}}$ is

$$u_{\mathrm{p_y}} = \frac{(\ddot{r}^{\mathrm{comm}}_{\mathrm{p_{y_d}}} - \boldsymbol{C}_{\mathrm{y}}\boldsymbol{A}^2\mathbb{X} + \begin{pmatrix} \omega^2_{\mathrm{n_y}} & 2\zeta_{\mathrm{y}}\omega_{\mathrm{n_y}} \end{pmatrix} \mathbf{e}_{\mathrm{y}})}{\boldsymbol{C}_{\mathrm{y}}\boldsymbol{A}\boldsymbol{B}_{\mathrm{y}}}$$

where

$$\boldsymbol{e}_{\mathrm{y}} = (e_{\mathrm{y}}, \dot{e}_{\mathrm{y}})^T$$

$$r^{\mathrm{comm}}_{\mathrm{p_{y_d}}} = \begin{pmatrix} 1 & 0 \end{pmatrix} \mathbf{z}_{\mathrm{y}}$$

where

$$\dot{\mathbf{z}}_{\mathrm{y}} = \begin{pmatrix} 0 & 1 \\ -\omega^2_{\mathrm{r_y}} & -2\zeta_{\mathrm{r_y}}\omega_{\mathrm{r_y}} \end{pmatrix} \mathbf{z}_{\mathrm{y}} + \begin{pmatrix} 0 \\ \omega^2_{\mathrm{r_y}} \end{pmatrix} r_{\mathrm{p_{y_d}}}(t)$$

$$r_{\mathrm{p_{y_d}}} = \tilde{r}_{\mathrm{p_{y_d}}} + r^{\mathrm{corr}}_{\mathrm{p_y}}$$

with

$$r^{\mathrm{corr}}_{\mathrm{p_y}} = K_{p_{\dot{\psi}}} e_{\dot{\psi}} + K_{i_{\dot{\psi}}} z_{\dot{\psi}} + K_{d_{\dot{\psi}}} \dot{e}_{\dot{\psi}} \qquad \text{where} \qquad \dot{z}_{\dot{\psi}} = e_{\dot{\psi}}$$

Putting all the parts together, we have

$$\begin{aligned} \dot{\mathbb{X}} &= \boldsymbol{A}\mathbb{X} + \boldsymbol{B}_{\mathrm{y}} u_{\mathrm{p_y}} \\ \dot{\mathbf{z}}_{\mathrm{y}} &= \begin{pmatrix} 0 & 1 \\ -\omega^2_{\mathrm{r_y}} & -2\zeta_{\mathrm{r_y}}\omega_{\mathrm{r_y}} \end{pmatrix} \mathbf{z}_{\mathrm{y}} + \\ &\quad + \begin{pmatrix} 0 \\ \omega^2_{\mathrm{r_y}} \end{pmatrix} (\tilde{r}_{\mathrm{p_{y_d}}} + K_{p_{\dot{\psi}}} e_{\dot{\psi}} + K_{i_{\dot{\psi}}} z_{\dot{\psi}} + K_{d_{\dot{\psi}}} \dot{e}_{\dot{\psi}}) \\ \dot{z}_{\dot{\psi}} &= \dot{\psi}_d - \dot{\psi} \end{aligned}$$

where

$$
\begin{aligned}
u_{\mathrm{p_y}} &= \frac{1}{\boldsymbol{C}_{\mathrm{y}}\boldsymbol{A}\boldsymbol{B}_{\mathrm{y}}}\left[\begin{pmatrix} 0 & 1 \end{pmatrix}\dot{\mathbf{z}}_{\mathrm{y}} - \boldsymbol{C}_{\mathrm{y}}\boldsymbol{A}^2\mathbb{X} + \begin{pmatrix} \omega_{\mathrm{n_y}}^2 & 2\zeta_{\mathrm{y}}\omega_{\mathrm{n_y}} \end{pmatrix}\begin{pmatrix} \begin{pmatrix} 1 & 0 \end{pmatrix}\mathbf{z}_{\mathrm{y}} - r_{\mathrm{p_y}} \\ \begin{pmatrix} 1 & 0 \end{pmatrix}\dot{\mathbf{z}}_{\mathrm{y}} - v_{\mathrm{p_y}} \end{pmatrix}\right] \\
&= \frac{1}{\boldsymbol{C}_{\mathrm{y}}\boldsymbol{A}\boldsymbol{B}_{\mathrm{y}}}\left[-\begin{pmatrix} \omega_{\mathrm{r_y}}^2 & 2\zeta_{\mathrm{r_y}}\omega_{\mathrm{r_y}} \end{pmatrix}\mathbf{z}_{\mathrm{y}} + \omega_{\mathrm{r_y}}^2[\tilde{r}_{\mathrm{p_{y_d}}} + \begin{pmatrix} K_{p_{\dot{\psi}}} & K_{d_{\dot{\psi}}} \end{pmatrix}\begin{pmatrix} e_{\dot{\psi}} \\ \dot{e}_{\dot{\psi}} \end{pmatrix} + K_{i_{\dot{\psi}}} z_{\dot{\psi}}]\right] \\
&\quad + \frac{1}{\boldsymbol{C}_{\mathrm{y}}\boldsymbol{A}\boldsymbol{B}_{\mathrm{y}}}\left[\begin{pmatrix} \omega_{\mathrm{n_y}}^2 & 2\zeta_{\mathrm{y}}\omega_{\mathrm{n_y}} \end{pmatrix}\mathbf{z}_{\mathrm{y}} - \begin{pmatrix} \omega_{\mathrm{n_y}}^2 & 2\zeta_{\mathrm{y}}\omega_{\mathrm{n_y}} \end{pmatrix}\begin{pmatrix} r_{\mathrm{p_y}} \\ v_{\mathrm{p_y}} \end{pmatrix} - \boldsymbol{C}_{\mathrm{y}}\boldsymbol{A}^2\mathbb{X}\right] \\
&= \frac{1}{\boldsymbol{C}_{\mathrm{y}}\boldsymbol{A}\boldsymbol{B}_{\mathrm{y}}}\left[\omega_{\mathrm{r_y}}^2\tilde{r}_{\mathrm{p_{y_d}}} + \omega_{\mathrm{r_y}}^2\begin{pmatrix} K_{p_{\dot{\psi}}} & K_{d_{\dot{\psi}}} \end{pmatrix}\begin{pmatrix} e_{\dot{\psi}} \\ \dot{e}_{\dot{\psi}} \end{pmatrix} - \begin{pmatrix} \omega_{\mathrm{n_y}}^2 & 2\zeta_{\mathrm{y}}\omega_{\mathrm{n_y}} \end{pmatrix}\begin{pmatrix} r_{\mathrm{p_y}} \\ v_{\mathrm{p_y}} \end{pmatrix}\right] \\
&\quad + \frac{1}{\boldsymbol{C}_{\mathrm{y}}\boldsymbol{A}\boldsymbol{B}_{\mathrm{y}}}\left[\begin{pmatrix} -1 & 1 \end{pmatrix}\begin{pmatrix} \omega_{\mathrm{r_y}}^2 & 2\zeta_{\mathrm{r_y}}\omega_{\mathrm{r_y}} \\ \omega_{\mathrm{n_y}}^2 & 2\zeta_{\mathrm{y}}\omega_{\mathrm{n_y}} \end{pmatrix}\mathbf{z}_{\mathrm{y}} + \omega_{\mathrm{r_y}}^2 K_{i_{\dot{\psi}}} z_{\dot{\psi}} - \boldsymbol{C}_{\mathrm{y}}\boldsymbol{A}^2\mathbb{X}\right]
\end{aligned}
$$

Define $\boldsymbol{C}_{\dot{\psi}}$ so that $\boldsymbol{C}_{\dot{\psi}}\mathbb{X} = \begin{pmatrix} e_{\dot{\psi}} \\ \dot{e}_{\dot{\psi}} \end{pmatrix}$ and $\boldsymbol{C}_{\mathrm{p_y}}$ so that $\boldsymbol{C}_{\mathrm{p_y}}\mathbb{X} = \begin{pmatrix} r_{\mathrm{p_y}} \\ v_{\mathrm{p_y}} \end{pmatrix}$.

Next, we shift the frozen equilibrium point $\mathbf{h}(\dot{\psi}_{\mathrm{d}}) = (\mathbb{X}_{\mathrm{eq}}^T, \mathbf{z}_{\mathrm{y_{eq}}}^T, z_{\dot{\psi}_{\mathrm{eq}}})^T$ to the origin to analyze stability. Define

$$(\acute{\mathbb{X}}^T, \acute{\mathbf{z}}_{\mathrm{y}}^T, \acute{z}_{\dot{\psi}})^T = (\mathbb{X}^T, \mathbf{z}_{\mathrm{y}}^T, z_{\dot{\psi}})^T - \mathbf{h}(\dot{\psi}_{\mathrm{d}})$$

The complete linearized equations are

$$
\begin{aligned}
\dot{\acute{\mathbb{X}}} &= \left[\boldsymbol{A} + \boldsymbol{B}_{\mathrm{y}}\frac{1}{\boldsymbol{C}_{\mathrm{y}}\boldsymbol{A}\boldsymbol{B}_{\mathrm{y}}}\left[\omega_{\mathrm{r_y}}^2\begin{pmatrix} K_{p_{\dot{\psi}}} & K_{d_{\dot{\psi}}} \end{pmatrix}\boldsymbol{C}_{\dot{\psi}} - \begin{pmatrix} \omega_{\mathrm{n_y}}^2 & 2\zeta_{\mathrm{y}}\omega_{\mathrm{n_y}} \end{pmatrix}\boldsymbol{C}_{\mathrm{p_y}} - \boldsymbol{C}_{\mathrm{y}}\boldsymbol{A}^2\right]\right]\acute{\mathbb{X}} \\
&\quad + \boldsymbol{B}_{\mathrm{y}}\frac{1}{\boldsymbol{C}_{\mathrm{y}}\boldsymbol{A}\boldsymbol{B}_{\mathrm{y}}}\left[\begin{pmatrix} -1 & 1 \end{pmatrix}\begin{pmatrix} \omega_{\mathrm{r_y}}^2 & 2\zeta_{\mathrm{r_y}}\omega_{\mathrm{r_y}} \\ \omega_{\mathrm{n_y}}^2 & 2\zeta_{\mathrm{y}}\omega_{\mathrm{n_y}} \end{pmatrix}\right]\acute{\mathbf{z}}_{\mathrm{y}} + \boldsymbol{B}_{\mathrm{y}}\frac{1}{\boldsymbol{C}_{\mathrm{y}}\boldsymbol{A}\boldsymbol{B}_{\mathrm{y}}}\omega_{\mathrm{r_y}}^2 K_{i_{\dot{\psi}}}\acute{z}_{\dot{\psi}} \\
\dot{\acute{\mathbf{z}}}_{\mathrm{y}} &= \begin{pmatrix} 0 \\ \omega_{\mathrm{r_y}}^2 \end{pmatrix}\begin{pmatrix} K_{p_{\dot{\psi}}} & K_{d_{\dot{\psi}}} \end{pmatrix}\boldsymbol{C}_{\dot{\psi}}\acute{\mathbb{X}} + \begin{pmatrix} 0 & 1 \\ -\omega_{\mathrm{r_y}}^2 & -2\zeta_{\mathrm{r_y}}\omega_{\mathrm{r_y}} \end{pmatrix}\acute{\mathbf{z}}_{\mathrm{y}} + \begin{pmatrix} 0 \\ \omega_{\mathrm{r_y}}^2 \end{pmatrix}K_{i_{\dot{\psi}}}\acute{z}_{\dot{\psi}} \qquad (13) \\
\dot{\acute{z}}_{\dot{\psi}} &= \begin{pmatrix} -1 & 0 \end{pmatrix}\boldsymbol{C}_{\dot{\psi}}\acute{\mathbb{X}}
\end{aligned}
$$

Consider $\acute{\boldsymbol{x}} = (\acute{\mathbb{X}}^T, \acute{\mathbf{z}}_{\mathrm{y}}^T, \acute{z}_{\dot{\psi}})^T$ as the new state vector of the system. The set of equations (13) is equivalent to

$$\dot{\acute{\boldsymbol{x}}} = \acute{\boldsymbol{A}}\acute{\boldsymbol{x}}$$

where the elements of $\acute{\boldsymbol{A}}$ are continuously differentiable functions of $\dot{\psi}_{\mathrm{d}} \in \Gamma = [0, a)$, where a is the maximum turn rate for the underwater glider. Suppose that $\acute{\boldsymbol{A}}$ is Hurwitz uniformly. This means the controller has been designed such that the closed-loop system is Hurwitz:

$$\mathrm{Re}[\lambda(\acute{\boldsymbol{A}})] \leq -\sigma < 0, \ \forall \ \dot{\psi}_{\mathrm{d}} \in \Gamma$$

Then, from Lemma 9.9 in [16] the Lyapunov equation

$$\mathbf{P}\acute{\boldsymbol{A}} + \acute{\boldsymbol{A}}^T\mathbf{P} = -\mathbb{I}.$$

has a unique positive definite solution $\mathbf{P}$ for every $\dot{\psi}_{\mathrm{d}} \in \Gamma$. $\mathbf{P}(\dot{\psi}_{\mathrm{d}})$ is continuously differentiable and satisfies

$$
\begin{aligned}
c_1\acute{\boldsymbol{x}}^T\acute{\boldsymbol{x}} \ \leq \ \acute{\boldsymbol{x}}^T\,\mathbf{P}(\dot{\psi}_{\mathrm{d}})\,\acute{\boldsymbol{x}} \ &\leq \ c_2\acute{\boldsymbol{x}}^T\acute{\boldsymbol{x}} \\
\|\frac{\partial}{\partial\dot{\psi}_{\mathrm{d}}}\mathbf{P}(\dot{\psi}_{\mathrm{d}})\| \ &\leq \ \vartheta
\end{aligned}
$$

for all $(\acute{\boldsymbol{x}}, \dot{\psi}_{\mathrm{d}}) \in \mathbb{R}^n \times \Gamma$, where c_1, c_2, and ϑ are positive constants independent of $\dot{\psi}_{\mathrm{d}}$. Consequently, the Lyapunov function $V(\acute{\boldsymbol{x}}, \dot{\psi}_{\mathrm{d}}) = \acute{\boldsymbol{x}}^T \mathbf{P}\, \acute{\boldsymbol{x}}$ satisfies the following inequalities

$$\begin{aligned} c_1\|\acute{\boldsymbol{x}}\|^2 &\leq V(\acute{\boldsymbol{x}}, \dot{\psi}_{\mathrm{d}}) \leq c_2\|\acute{\boldsymbol{x}}\|^2 \\ \|\frac{\partial V}{\partial \acute{\boldsymbol{x}}}\| g(\acute{\boldsymbol{x}}, \dot{\psi}_{\mathrm{d}}) &\leq -c_3\|\acute{\boldsymbol{x}}\|^2 \\ \|\frac{\partial V}{\partial \acute{\boldsymbol{x}}}\| &\leq c_4\|\acute{\boldsymbol{x}}\| \\ \|\frac{\partial V}{\partial \dot{\psi}_{\mathrm{d}}}\| &\leq c_5\|\acute{\boldsymbol{x}}\|^2 \end{aligned}$$

for all $\acute{\boldsymbol{x}} \in D = \{\acute{\boldsymbol{x}} \in \mathbb{R}^n | \|\acute{\boldsymbol{x}}\| < r\}$ and $\dot{\psi}_{\mathrm{d}} \in \Gamma = [0, a)$ where, once again, a is the maximum turn rate for the underwater glider. The positive constants in inequalities are: $c_1 = \lambda_{\min}(\mathbf{P})$, $c_2 = \lambda_{\max}(\mathbf{P})$, $c_3 = 1$, $c_4 = 2\lambda_{\max}(\mathbf{P})$, and $c_5 = 0$ (Lemma 9.9 in [16]). The solutions are uniformly ultimately bounded with an ultimate bound proportional to ε, the upper bound of the turn acceleration. The upper bound of ε can be calculated from the following relation:

$$\| \ddot{\psi}_{\mathrm{d}}(t) \| \leq \varepsilon < \frac{c_1 c_3}{c_2} \times \frac{r}{r c_5 + c_4 L}\,, \quad \|\frac{\partial \mathbf{h}}{\partial \dot{\psi}_{\mathrm{d}}}\| \leq L \quad (14)$$

The norm of the tracking error remains smaller than $k\varepsilon$ for some finite $k > 0$. Moreover, if $\ddot{\psi}_{\mathrm{d}}(t) \to 0$ as $t \to \infty$, the tracking error tends to zero by Theorem 9.3 in [16].

Solving the Lyapunov equation and calculating the eigenvalues of $\mathbf{P}$ one obtains the c_i, $i = 1, 2, \ldots, 5$ and an upper bound for ε, the limit for commanded turn accelerations. Applying the proposed motion control system to the *Slocum* model given in [2], and performing the analysis outlined above, one obtains the constants:

$$c_1 = \lambda_{\min}(\mathbf{P}) = -378.75, \;\; c_2 = \lambda_{\max}(\mathbf{P}) = 979.82,$$
$$c_3 = 1, \;\; c_4 = 2\lambda_{\max}(\mathbf{P}), \;\; \text{and} \;\; c_5 = 0.$$

which gives

$$|\ddot{\psi}_{\mathrm{d}}(t)| \leq \varepsilon < 2 \times 10^{-4} \frac{r}{L}$$

This is a conservative upper bound for acceleration in turn rate reference commands. A relaxed bound could be obtained by applying similar analysis in the time varying setting. (See Theorems 7.4 and 7.8 in [25], for example.)

7 Simulation Results

A sophisticated glider model based on the *Slocum* model given in [2] was linearized about the following equilibrium flight condition, which corresponds to wings-level, descending flight:

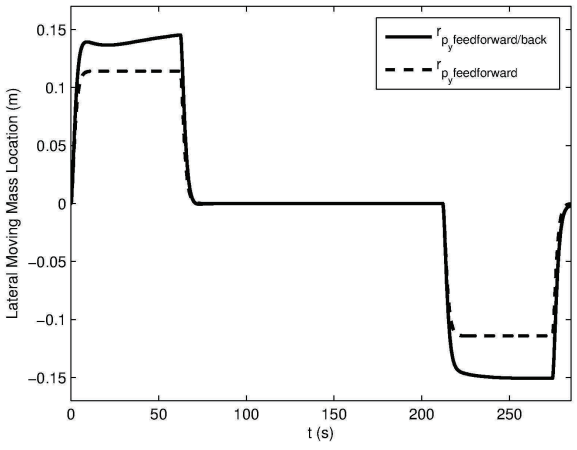

Figure 4. Lateral moving mass location (open- and closed-loop).

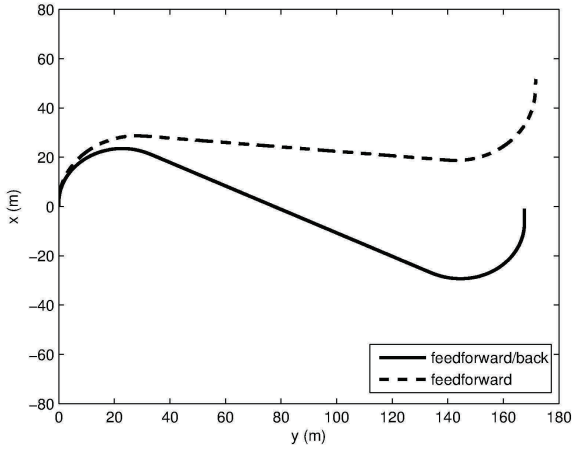

Figure 5. *Slocum* path in response to input histories shown in Figure 4.

$$V_0 = 0.77 \text{ m/s}, \qquad \alpha_0 = 4.3^\circ,$$
$$\theta_0 = -8.4^\circ, \qquad \gamma_0 = -12.7^\circ, \qquad \text{and} \qquad \tilde{m}_0 = 0.63 \text{ kg}.$$

The moving mass values are $m_{\mathrm{p_x}} = m_{\mathrm{p_y}} = 9$ kg. The servo-actuator parameter values are

$$\omega_{\mathrm{n_x}} = 20 \text{ rad/s}, \qquad \zeta_{\mathrm{x}} = 0.001, \qquad \omega_{\mathrm{r_x}} = 0.8 \text{ rad/s}, \quad \text{and} \qquad \zeta_{\mathrm{r_x}} = 1$$
$$\omega_{\mathrm{n_y}} = 20 \text{ rad/s}, \qquad \zeta_{\mathrm{y}} = 0.01, \qquad \omega_{\mathrm{r_y}} = 0.8 \text{ rad/s}, \quad \text{and} \qquad \zeta_{\mathrm{r_y}} = 1$$

The PID control parameter values are

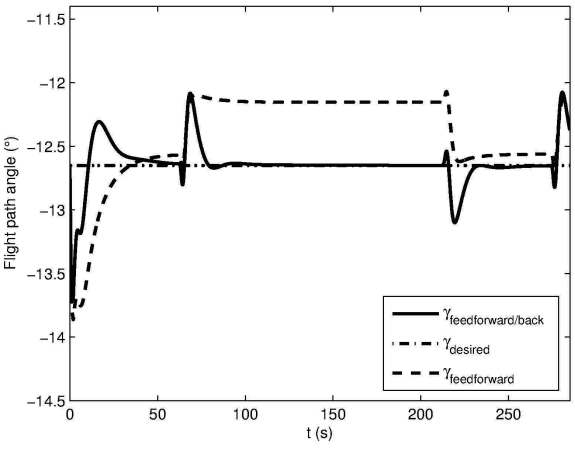

Figure 6. Glide path angle response to command sequence.

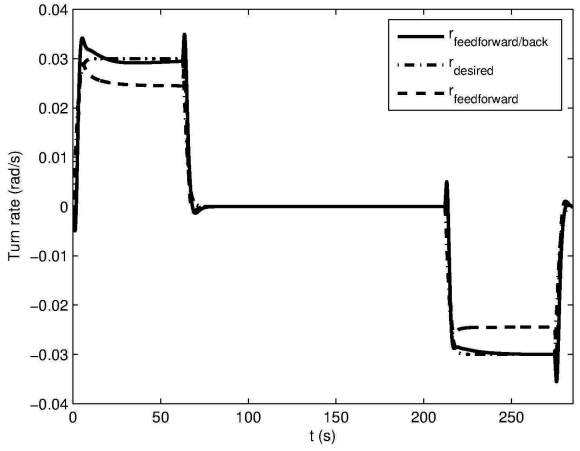

Figure 7. Turn rate response to command sequence.

$$K_{p_\gamma} = -0.2 \text{ m}, \qquad T_{i_\gamma} = 2.3 \text{ s},$$
$$\text{and} \qquad T_{d_\gamma} = 2 \text{ s}$$
$$K_{p_{\dot\psi}} = 0.2 \text{ m/(rad/s)}, \qquad T_{i_{\dot\psi}} = 0.65 \text{ s},$$
$$\text{and} \qquad T_{d_{\dot\psi}} = 0.39 \text{ s}$$

Figures 4 through 8 compare the results of simulations using feedforward and feedforward/feedback control. Figure 4 shows the lateral mass location in response to a command sequence that is intended to effect a right turn, a straight segment, and a left turn (viewed from above) from an initial point to a desired final point. In the open-loop case (feedforward only), the moving mass is simply commanded to move to the (approximate) equilibrium value corresponding to a desired heading rate $\dot\psi_{\text{d}}$. In the closed-loop case (feedforward/feedback), however, the heading rate is directly commanded, with the lateral moving mass actuator responding as necessary. The resulting path is depicted in Figure 5.

Figures 6 and 7 show desired, open-loop, and closed-loop value of the vehicle's glide path angle and turn rate. As expected, the deviation between the open-loop values and the desired values is significant. In Figure 7, the small spikes at the end of each segment correspond to reaction forces due to the movement of the lateral mass within the vehicle. We note that the turn rate magnitudes are of the same order as turn rates seen in glider operations. The *Slocum* glider, for example, can achieve a 20-30 m turn radius at speeds on the order of 0.5 m/s. A shallow-water variant of *Slocum*, which includes a movable rudder, can perform turns with a 7 m radius [4]. Figure 8 shows the location of the longitudinal moving mass, which regulates the glide path angle.

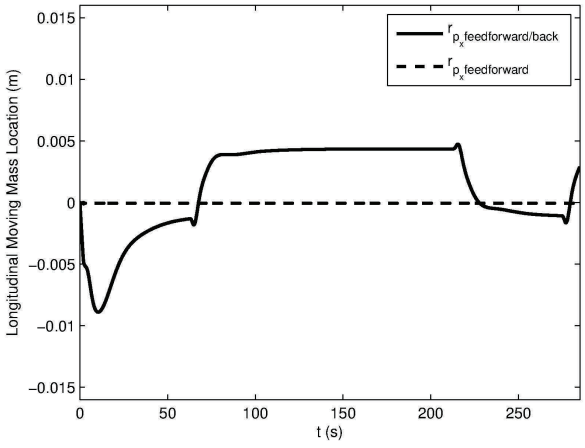

Figure 8. Variation in longitudinal moving mass position from nominal.

Remark 7.1. *The path in Figure 5 is reminiscent of a Dubins path, although the vehicle and actuator dynamics are included here. Time-optimal paths for a Dubins car with acceleration limits are discussed in [17] and [26], where it is recognized that extremal paths comprise sequences of straight, clothoidal, and circular segments. We call these "suboptimal Dubins paths."*

It must be stressed that the final guidance loop has not been closed, at this point. That is, we have not presented a control law to make the vehicle track a commanded *path*, such as a suboptimal Dubins path. Rather, we have presented the underlying motion control system over which a guidance loop might be imposed.

Figures 9 through 11 compare results of the simulation for the common feedback motion control system and the feedforward/feedback motion control system presented in this work. Figure 9 shows that the steady-motion based feedforward/feedback system reaches the desired turn rate

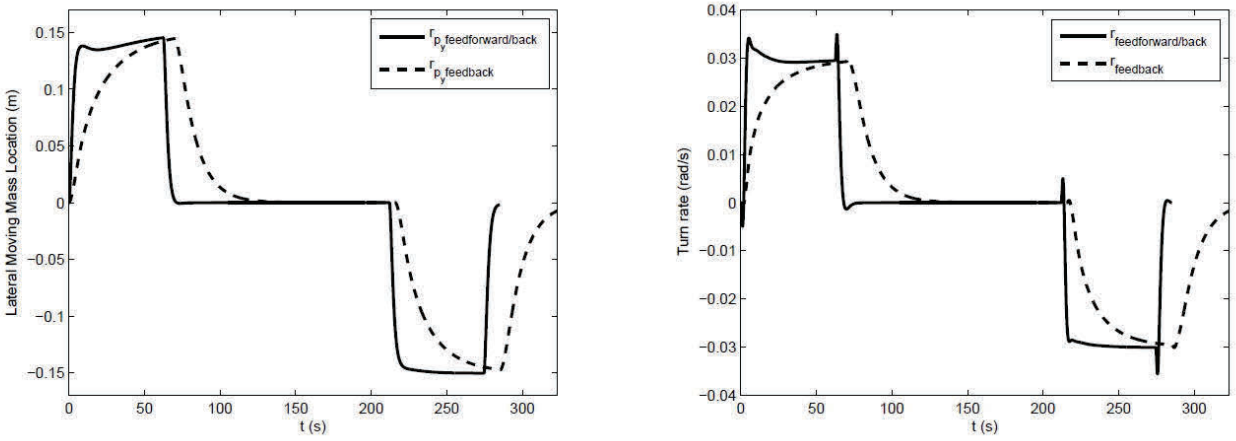

Figure 9. Lateral moving mass position and turn rate.

much faster. Hence, the vehicle reaches the desired final point in shorter time (Figure 11). Figure 10 illustrates the effectiveness of both control loops in maintaining a constant flight path angle.

Comparing results of the simulations, for the three cases of feedforward, feedback, and feedforward/feedback controller, shows that there is large error in turn rate when using just feedforward controller (Figure 7) which corresponds to large error in the resultant path (Figure 5). Figure 11 shows that the feedback controller is slow but precise, therefore it takes longer time and larger distance to achieve the desired turn rate (Figure 11). The combination, the proposed feedforward/feedback controller, illustrates fast, precise tracking of the commanded turn rate. Since the control system relies largely on steady motions, it is intrinsically efficient.

8 Conclusions

Building on prior results in glider steady motion analysis, a feedforward/feedback motion control system was presented to control speed, glide path angle, and turn rate. The control system uses feedforward commands obtained from an approximate solution for steady turning motion and includes feedback to compensate for approximation error and other uncertainties. The control system design includes model reference controllers for the servo-actuators, to allow actuator rate and magnitude saturation effects to be more easily analyzed and accommodated. Stability of the closed-loop system was analyzed using slowly varying systems theory in which the turn rate command was treated as a slowly varying parameter. A bound on turn acceleration was obtained as a product of the analysis. The controller's effectiveness was demonstrated in a simulation of a multi-body model of the underwater glider *Slocum*.

The proposed control system provides a mechanism for path following. The next step is to implement a guidance strategy, together with a path planning strategy, and one which continues to exploit the natural efficiency of this class of vehicle. The structure of the approximate solution for steady turning motion is such that, to first order in turn rate, the glider's horizontal component of motion matches that of the "Dubins car," a simple model for a wheeled robot that moves at constant speed and can turn left or right, up to some turn rate limit. The Dubins car is a classic example in the study of time-optimal control for mobile robots. For an underwater glider, one can relate time optimality to energy optimality. Specifically, for an underwater glider travelling at a constant speed and maximum flight efficiency (i.e., the maximum lift-to-drag ratio, in still water), minimum time paths are minimum energy paths. Hence, energy-efficient paths can be obtained by generating sequences of steady wings-level and turning motions. These efficient paths can, in turn, be followed using the motion control system described here.

In closing, we note that the feedforward component of the proposed control system, as presented, relies on the analytical solution for the steady turning motions of an underwater glider. This analysis is based on a sophisticated model of the underwater glider dynamics. In the absence of such a model, and the corresponding solution for steady motions, one may instead use a look-up table which maps vehicle configurations to stable, steady motions. Although such a table would have to be developed through an exhaustive series of experimental sea trials, the approach may, in some cases, be more expedient than developing a complete dynamic model.

Acknowledgements

This work was supported by the Office of Naval Research under grant number N00014-08-1-0012.

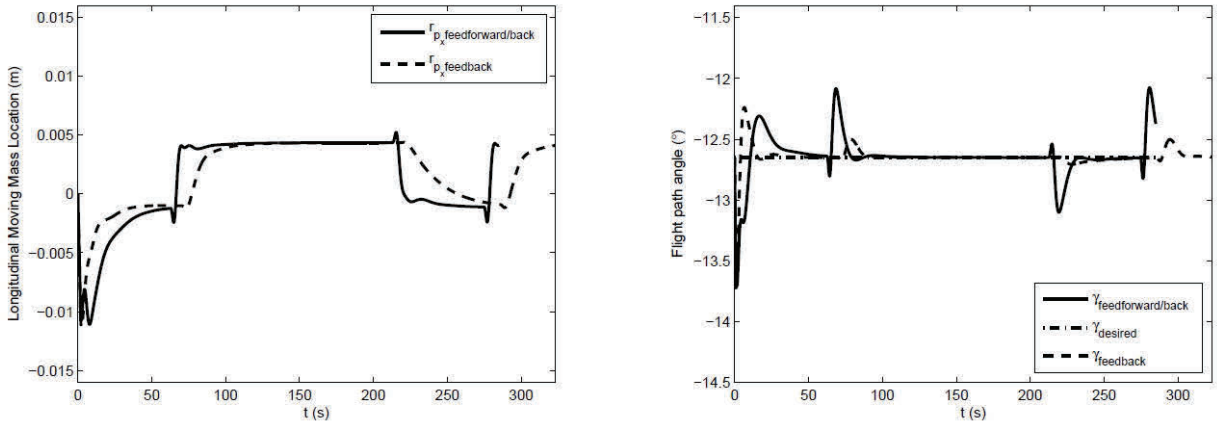

Figure 10. Longitudinal moving mass position and flight path angle.

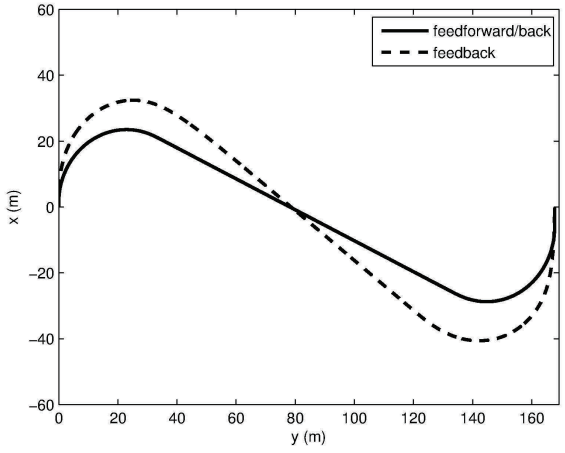

Figure 11. *Slocum* path in response to feedback and feedforward/feedback compensator.

References

[1] R. Bachmayer, J.G. Graver, and N. E. Leonard. Glider control: A close look into the current glider controller structure and future developments. In *IEEE Oceans 2003*, volume 2, pages 951–954, 2003.

[2] P. Bhatta. *Nonlinear Stability and Control of Gliding Vehicles*. PhD thesis, Princeton University, 2006.

[3] B. Chen and D. Pompili. Uncertainty-aware localization solution for under-ice autonomous underwater vehicles. Seoul, Korea, 2012. 2012 9th Annual IEEE Communications Society Conference on Sensor, Mesh and Ad Hoc Communications and Networks.

[4] R. E. Davis, C. C. Eriksen, and C. P. Jones. Autonomous buoyancy-driven underwater gliders. In G. Griffiths, editor, *Technology and Applications of Autonomous Underwater Vehicles*, volume 2, chapter 3. Taylor and Francis, 2002.

[5] C. C. Eriksen, T. J. Osse, R. D. Light, T. Wen, T. W. Lehman, P. L. Sabin, J. W. Ballard, and A. M. Chiodi. Seaglider: A long-range autonomous underwater vehicle for oceanographic research. *Journal of Oceanic Engineering*, 26(4):424–436, 2001. Special Issue on Autonomous Ocean-Sampling Networks.

[6] S. Fan, A. Wolek, and C. A. Woolsey. Stability and performance of underwater gliders. Hampton Roads, VA, October 14-19 2012. OCEANS 2012 IEEE/MTS.

[7] T. I. Fossen. *Guidance and Control of Ocean Vehicles*. John Wiley and Sons, 1995.

[8] A. M. Galea. Optimal path planning and high level control of an autonomous gliding underwater vehicle. Master's thesis, Massachusetts Institute of Technology, 1999.

[9] J. S. Geisbert. Hydrodynamic modeling for autonomous underwater vehicles using computational and semi-empirical methods. Master's thesis, Virginia Polytechnic Institute & State University, Blacksburg, VA, June 2007.

[10] J. G. Graver. *Underwater Gliders: Dynamics, Control, and Design*. PhD thesis, Princeton University, 2005.

[11] J. G. Graver, J. Liu, C. A. Woolsey, and N. E. Leonard. Design and analysis of an underwater glider for controlled gliding. In *Conference on Information Sciences and Systems*, pages 801–806, 1998.

[12] J. Guckenheimer and P. Holmes. *Nonlinear Oscillations, Dynamical Systems, and Bifurcations of Vector Fields*. Springer-Verlag, New York, NY, 1983.

[13] P. Hartman. *Ordinary Differential Equations*. John Wiley and Sons, Inc., New York, NY, 1964.

[14] S. A. Jenkins, D. E. Humphreys, J. Sherman, J. Osse, C. Jones, N. Leonard, J. Graver, R. Bachmayer, T. Clem, P. Carroll, P. Davis, J. Berry, P. Worley, and J. Wasyl. Underwater glider system study. Technical Report 53, Scripps Institution of Oceanography, May 2003.

[15] C. Jones, D. Webb, S. Glenn, O. Schofield, J. Kerfoot, J. Kohut, H. Roarty, D. Aragon, C. Haldeman, T. Haskin, and A. Kahl. Slocum glider extending the endurance. Durham, NH, August 23-26 2009. The 16th International Symposium on Unmanned Untethered Submersible Technology (UUST09).

[16] H. K. Khalil. *Nonlinear Systems*. Prentice Hall, Upper Saddle River, NJ, third edition, 2002.

[17] V. Kostov and E. Degtiariova-Kostova. Suboptimal paths in the problem of a planar motion with bounded derivative of the curvature. Technical Report 2051, Institut National de Recherche en Informatique et en Automatique (INRIA), July 1993.

[18] N. E. Leonard and J. G. Graver. Model-based feedback control of autonomous underwater gliders. *Journal of Oceanic Engineering*, 26(4):633–645, 2001. Special Issue on Autonomous Ocean-Sampling Networks.

[19] Naomi Ehrich Leonard, Derek A. Paley, Russ E. Davis, David M. Fratantoni, Francois Lekien, and Fumin Zhang. Coordinated control of an underwater glider fleet in an adaptive ocean sampling field experiment in monterey bay. *J. Field Robotics*, 27(6):718–740, 2010.

[20] N. Mahmoudian, J. Geisbert, and C. A. Woolsey. Approximate analytical turning conditions for underwater gliders: Implications for motion control and path planning. *IEEE Journal of Oceanic Engineering*, 35(1):131 – 143, 2010.

[21] N. Mahmoudian and C. Woolsey. Analysis of feedforward/feedback control design for underwater gliders based on slowly varying systems theory. Chicago, IL, Aug 20-23 2009. AIAA Guidance, Navigation and Control Conference and Exhibit.

[22] N. Mahmoudian, C. Woolsey, and J. Geisbert. Steady turns and optimal paths for underwater gliders. Hilton Head, SC, Aug 20-23 2007. AIAA Guidance, Navigation and Control Conference and Exhibit.

[23] N. Mahmoudian and C. A. Woolsey. Underwater glider motion control. In *IEEE Conference on Decision and Control*, pages 552 – 557, Cancun, Mexico, December 2008.

[24] C. Peterson and D. A. Paley. Multivehicle coordination in an estimated time-varying flowfield. *AIAA J. Guidance, Control, and Dynamics*, 34(1):177–191, 2011.

[25] W. J. Rugh. *Linear System Theory*. Prentice Hall, Upper Saddle River, NJ, second edition, 1996.

[26] A. Scheuer and Ch. Laugier. Planning sub-optimal and continuous-curvature paths for car-like robots. In *IEEE/RSJ International Conference on Intelligent Robots and Systems*, pages 25–31, Victoria, B.C., Canada, October 1998.

[27] J. Sherman, R. E. Davis, W. B. Owens, and J. Valdes. The autonomous underwater glider "Spray". *Journal of Oceanic Engineering*, 26(4):437–446, 2001. Special Issue on Autonomous Ocean-Sampling Networks.

[28] X. Tan, W. Xi, and J. S. Baras. Decentralized coordination of autonomous swarms using parallel gibbs sampling. *Automatica*, 46(12):2068–2076, 2010.

[29] L. Techy, K. A. Morganseny, and C. A. Woolsey. Long-baseline acoustic localization of the seaglider underwater glider. San Francisco, CA, June 29 - July 1 2011. 2011 American Control Conference.

[30] D. C. Webb, P. J. Simonetti, and C. P. Jones. SLOCUM: An underwater glider propelled by environmental energy. *Journal of Oceanic Engineering*, 26(4):447–452, 2001. Special Issue on Autonomous Ocean-Sampling Networks.

[31] A. Wolek, J. Burns, C. A. Woolsey, J. Quezer, L. Techy, and K. Morgansen. A maneuverable, pneumatic underwater glider. Hampton Roads, VA, October 14-19 2012. OCEANS 2012 IEEE/MTS.

[32] C. A. Woolsey. Reduced Hamiltonian dynamics for a rigid body/mass particle system. *Journal of Guidance, Control, and Dynamics*, 28(1):131–138, January-February 2005.

[33] F. Zhang, J. Thon, C. Thon, and X. Tan. Miniature underwater glider: Design, modeling, and experimental results. Saint Paul, Minnesota, May 14-18 2012. 2012 IEEE International Conference on Robotics and Automation.

[34] F. Zhang, F. Zhang, and X. Tan. Steady spiraling motion of gliding robotic fish. Vilamoura, Algarve, Portugal, October 7-12 2012. 2012 IEEE/RSJ International Conference on Intelligent Robots and Systems.